Passive UHF-RFID Technology: Integrated Communication, Localization and Sensing

Andrea Motroni, *Member, IEEE*, Glauco Cecchi, *Student Member, IEEE*, Andrea Ria, *Senior Member, IEEE*, and Paolo Nepa, *Senior Member, IEEE*

***Abstract*—This paper presents an environmental mapping system based on passive Internet of Things (IoT) nodes implemented through Ultra High-Frequency (UHF) Radio Frequency IDentification (RFID) devices with sensing capabilities. An RFID sensor tag provides environmental information as temperature, humidity, lighting, etc. aside its unique identifier. The paper focuses on creating a detailed map of indoor facilities like buildings, warehouses, or plants by combining location information with sensing data. To achieve accurate positioning with passive RFID devices, the paper employs techniques based on the Synthetic Aperture Radar (SAR) method. This method utilizes the phase of the backscattering signal and the relative motion between the reading antenna and the targeted devices, which can be implemented by a mobile robot. The paper includes a demonstrator that showcases the aforementioned system. Passive RFID sensor tags capable of monitoring temperature are deployed in an indoor scenario, whereas a moving antenna implements the SAR method. The results demonstrate localization errors within a few centimeters. The paper also presents criteria for selecting trajectories that may improve localization accuracy. Furthermore, the paper evaluates the actual capabilities of commercial passive RFID sensors.**

***Index Terms*—UHF-RFID, synthetic aperture radar, UHF-RFID localization, sensing, RFID sensors, radiolocalization, environmental sensing.**

I. Introduction

PASSIVE backscattering communications at the Ultra High Frequency (UHF) band are a promising solution to avoid battery management issues in Internet of Things (IoT) applications [1], [2]. Indeed, Radio Frequency IDentification (RFID) technology represents the ideal candidate for automatic product tracking, warehouse management, food monitoring etc. [3]. However, the absence of a battery makes the link budget unbalanced at the reader side, which must deliver higher power with respect to systems with active nodes. Nevertheless, an architecture with a single active device along with a multitude of passive devices may be easier to manage than multiple active nodes.

UHF-RFID are increasingly becoming IoT nodes thanks to sensing capabilities integrated on the device aside the Radio Frequency (RF) communication [4]. Recently, passive UHF-RFID sensor tags have been spreading in literature and market for a manifold of applications [5], [6], [7], [8], [9], [10], [11], [12], [13]. A review of these technologies can be found in [14].

Moreover, location-aware communications are becoming relevant in 5G scenarios and indoor environments. An IoT framework comprising sensor nodes that can be easily located within a target environment may represent an appealing solution for environmental mapping, namely to create temperature, humidity, lighting or gas exposure maps inside of a given building, plant, warehouse or any other facility [15] to come out with a valuable "Digital Twin" of the indoor environment [16]. Indeed, the low cost of passive tags allows a large-scale deployment of devices for enhancing the monitoring features.

The localization of UHF-RFID passive tags has been deeply explored in the last decade [17], [18], [19], [20]. Among localization algorithms and techniques, phase-based solutions [21] have become popular since the phase of the tag backscattered signal is a sensitive and promising parameter to provide location-related data.

Although subject to several issues as phase offsets [22], phase cyclicity, multipath, or antenna phase center displacements [23] in presence of nearby objects, phase-based localization techniques can be upgraded to Synthetic Aperture Radar (i.e., SAR) localization schemes which might mitigate above issues and which have been widely proved to allow for few tens of centimeters position errors [24], [25], [26], [27], [28], [29], [30].

From an architectural point of view, we can figure out static RFID sensor tags and one or more moving reader antennas which travel in the environment and gather at the same time both phase of the tag backscattered signal and sensor data. When a sufficient localization accuracy is available, an environmental map of the target area giving environmental parameters info correlated with timestamps and locations is possible. RFID tags changing their locations can be detected

Manuscript received 6 May 2023; revised 11 July 2023; accepted 28 July 2023. Date of publication 4 August 2023; date of current version 3 October 2023. This work was supported in part by the PARTITALIA srl within the Project MONITOR (A Cyber Physical System for the Automatic and Real-Time Monitoring of Items in Industrial Scenarios and Large Warehouses – CUP) under Grant B41B20000330005 in the framework of "Fund for Sustainable Growth – Smart factory" PON I&C 2014-2020, D.M. 5 March 2018, and in part by the Italian Ministry of University and Research (MUR) in the framework of both the CrossLab Project (Departments of Excellence) and the FoReLab Project (Departments of Excellence). *(Corresponding author: Andrea Motroni.)*

Andrea Motroni, Glauco Cecchi, and Andrea Ria are with the Department of Information Engineering, University of Pisa, 56122 Pisa, Italy (e-mail: andrea.motroni@unipi.it).

Paolo Nepa is with the Department of Information Engineering, University of Pisa, 56122 Pisa, Italy, and also with the Institute of Electronics, Computer and Telecommunication Engineering, Italian National Research Council, 10135 Turin, Italy.

Digital Object Identifier 10.1109/JRFID.2023.3301093

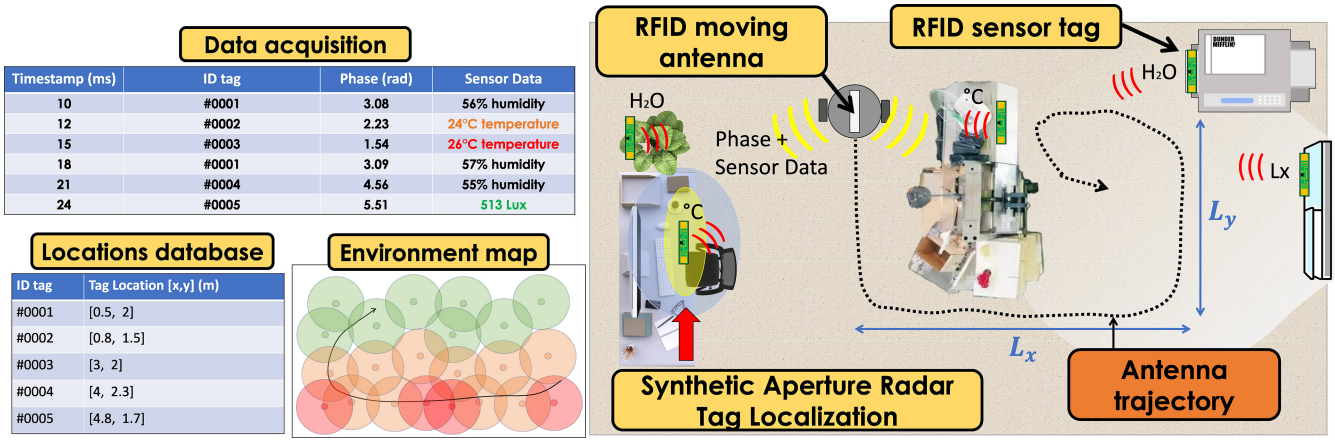

Fig. 1. Schematic of the proposed system for integrated localization and sensing. A RFID moving antenna travels in the scenario, describing an $L_x \times L_y$ synthetic array to localize the target RFID sensor tags and create an environmental map with tag locations and sensor outputs.

again in a second SAR run to update the map. This concept is represented graphically in Figure 1.

One of the advantages of a location system based on synthetic aperture is that it eliminates the requirement for a fixed and wide reader infrastructure. This characteristic prevents scalability issues and excessive costs when covering large areas. Furthermore, the method employed in this study operates independently of the specific tag utilized and does not necessitate the presence of reference tags.

This paper presents a proof-of-concept of the aforementioned system. Commercial-Off-The-Shelf (COTS) passive RFID sensor tags are deployed in a room and interrogated by a moving antenna acquiring simultaneously temperature data and phase data for localization. 2D SAR processing is used to estimate tag locations. Few cm localization error and reliable temperature data are acquired.

It is important to mention that the localization and sensing operations in this system are independent of each other. What sets this system apart is its novel approach of integrating these two operations within a simple RFID-based infrastructure that is both cost-effective and easily accessible.

This paper is organized as follows. Section II presents the SAR localization algorithm, Section III describes the experimental setup and used hardware. Section IV shows the obtained results, and Section V draws conclusions and briefly introduces future works.

II. SAR Localization Method in the 2D Domain

SAR-based localization of RFID tags has been implemented through a variety of algorithms [24], [25], [26], [27], [28], [29], [30]. These methods perform similarly to Maximum Likelihood (ML) estimators [31], especially for high values of Signal-to-Noise-Ratio (SNR). One of the most popular techniques involves phase normalization and the transformation to the phasor domain [32], and it is summarized below.

Let us assume that a moving antenna at fixed height z_{ant} travels inside a given area by describing a 2D trajectory. From the theoretical background of SAR localization methods for RFID tags, it is well known that localization performance is related to the size of the synthetic aperture, i.e., the length of the moving antenna path [24], [25], [26], [27], [28], [29], [30]. Usually, accurate localization on the xy-plane (2D domain) requires a sufficiently wide planar antenna motion along two orthogonal directions. In other words, the motion along the x- and y-axes influence the localization error on the x- and y-coordinates, respectively. Antenna motion can be made by using handling systems, mobile robots, drones, or other vehicles. We assume that the height of target RFID tags is known and constant.

We suppose that a RFID sensor tag is placed at $\mathbf{p_{tag}} = [x_{tag}, y_{tag}, z_{tag}]^T$. Such tag is detected N_R times by the reader, where N_R coincides with the number of antenna consecutive locations. The antenna location at the k-th timestep is $\mathbf{p_k} = [x_k, y_k, z_k]^T$, with $k = [0, \ldots, N_R - 1]$. The moving antenna forms a synthetic array whose sizes are defined as $L_x = \max(x_k) - \min(x_k)$, $L_y = \max(y_k) - \min(y_k)$, and $L_z = 0$ m, being the height fixed (see Fig. 1).

At the k-th timestep, the reader antenna gets a noisy phase sample $\hat{\phi}_k$:

$$\hat{\phi}_k = \mathrm{mod}\left(\frac{-4\pi \|\mathbf{p_k} - \mathbf{p_{tag}}\|_2}{\lambda} + \phi_{off} + w_k, 2\pi\right) \quad (1)$$

where mod is the remainder of integer division, $\|\cdot\|_2$ is the Euclidean distance operator, λ is the carrier wavelength, ϕ_{off} is a phase offset which takes in account cables, antenna and tag circuitry and polarization mismatches and it is assumed as a slowly varying effect [33]. w_k is a normal random variable defined as $w_k \sim \mathcal{N}(0, \sigma_w^2)$ where σ_w is the noise standard deviation. Since the phase is a periodic quantity, the reader can detect it only with a 2π–periodicity. The offset term ϕ_{off} is unknown a-priori and hard to calibrate [22], so that to release from it, a phase variation with respect to the first available sample (here indicated for simplicity with $k = 0$) is computed by the following $\Delta\hat{\phi}_k = \hat{\phi}_k - \hat{\phi}_0$.

The normalized measured phase sequence is then organized in a phasors vector denoted as $\mathbf{a}$:

$$\mathbf{a} = \left[1, \ldots, e^{j\Delta\hat{\phi}_k}, \ldots, e^{j\Delta\hat{\phi}_{N_R}}\right]^T \quad (2)$$

To estimate the tag coordinates, the method creates a matching function $\mathbf{C}(\mathbf{p}'_{\mathbf{tag}})$ depending on a hypothetical tag location

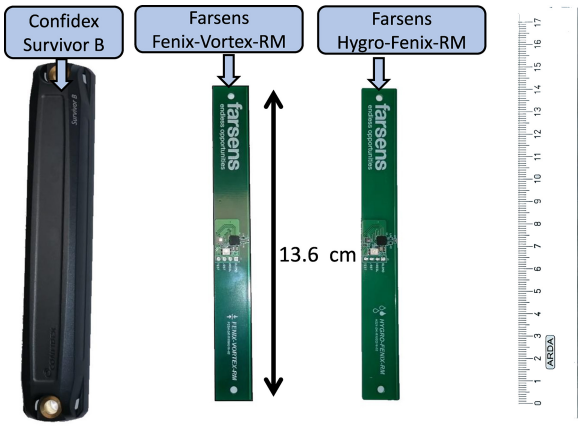

Fig. 2. Sensor RFID tags used for the experiments: Farsens EVAL02–Hygro–Fenix–RM, Farsens EVAL02–Fenix–Vortex–RM, and Confidex Survivor B.

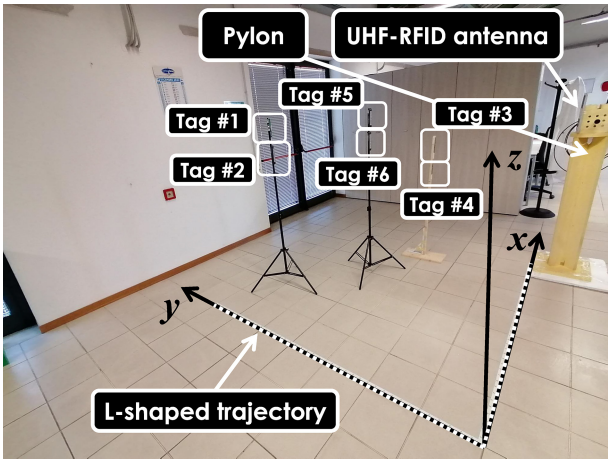

Fig. 3. Experimental setup at University of Pisa facilities.

$\mathbf{p}_{\mathbf{tag}}^{'}$. The estimated tag location is then retrieved through the maximization of the matching function argument (i.e., best fitting hypothetical tag coordinates):

$$\hat{\mathbf{p}}_{\mathbf{tag}} = \arg\max_{\mathbf{p}_{\mathbf{tag}}^{'}} \mathbf{C}(\mathbf{p}_{\mathbf{tag}}^{'}) \tag{3}$$

The calculation of $\mathbf{C}(\mathbf{p}_{\mathbf{tag}}^{'})$ is as follows. For each hypothetical tag location $\mathbf{p}_{\mathbf{tag}}^{'}$, the noiseless theoretical model of $\Delta\hat{\phi}_k$ is calculated and denoted $\Delta\phi_k(\mathbf{p}_{\mathbf{tag}}^{'})$. Then, a set of phasors vectors $\mathbf{b}(\mathbf{p}_{\mathbf{tag}}^{'})$ is computed through:

$$\mathbf{b}\left(\mathbf{p}_{\mathbf{tag}}^{'}\right) = \left[1, \ldots, e^{j\Delta\phi_k\left(\mathbf{p}_{\mathbf{tag}}^{'}\right)}, \ldots, e^{j\Delta\phi_{N_R}\left(\mathbf{p}_{\mathbf{tag}}^{'}\right)}\right]^T \tag{4}$$

Then:

$$\mathbf{C}(\mathbf{p}_{\mathbf{tag}}^{'}) = \frac{\left|\mathbf{a}^H\mathbf{b}\left(\mathbf{p}_{\mathbf{tag}}^{'}\right)\right|}{\|\mathbf{a}\|_2\left\|\mathbf{b}\left(\mathbf{p}_{\mathbf{tag}}^{'}\right)\right\|_2} \tag{5}$$

This function is normalized and, therefore, spans from 0 to 1.

It is required that two consecutive antenna positions are spaced less than $\lambda/4$ to satisfy the sampling theorem and avoiding the occurrence of grating lobes in the matching function [26]. This must be carefully accounted when designing the antenna trajectory as well as antenna speed and reader interrogation interval.

III. Experimental Setup

In environments such as the food industry or greenhouses, monitoring room temperature is essential for proper food preservation [11]. We tested three typologies of RFID tags with embedded electronic sensors: Farsens EVAL02–Hygro–Fenix–RM, Farsens EVAL02–Fenix–Vortex–RM, and Confidex Survivor B (shown in Fig. 2). All tags support the BAP (Battery Assisted Passive) mode but are here configured in passive mode. Farsens EVAL02–Hygro–Fenix–RM and Farsens EVAL02–Fenix–Vortex–RM include a dipole antenna and are compliant with EPC C1G2 RFID COTS readers. They present a reading range of around 5 m at 2 W ERP. Sensor tag architecture is composed by a RFID chip (Rocky IC 100 by Farsens, sensitivity –14 dBm in passive mode), a microcontroller, and an external sensor [34].

Farsens EVAL02–Hygro–Fenix–RM is equipped with a HTS221 temperature sensor manufactured by ST Microelectronics with a −40°C to 85°C temperature range and a ±1°C accuracy. The Farsens EVAL02–Fenix–Vortex–RM is equipped with a LPS25H temperature sensor by ST Microelectronics with −30°C to 85°C temperature range and ±2°C accuracy.

Confidex Survivor B is a sensor tag designed for metallic surfaces encapsulated in a plastic coverage. It embeds the EM4325 EM Microelectronics chip (sensitivity from –7 to –9 dBm in passive mode). The embedded temperature sensor supports a temperature range of −40°C to 60°C with a typical accuracy of ±1°C.

As in Fig. 3, an experimental environment was set-up with a UHF-RFID antenna that is moved along a "L-shaped" trajectory of $L_x \times L_y$ size ($L_x = L_y = 2.1$ m).

An Impinj R420 RFID reader is connected to a Times-7 SlimLine A4030C Right Hand Circular Polarization (RHCP) patch antenna with $G_r = 6.5$ dBi and HPBW = 60° (Half Power Beam Width) on both vertical and horizontal planes. The reader provides a power $P_{TX} = 28$ dBm to the antenna through a 3-m coaxial cable at the frequency of 865.7 MHz (European Telecommunications Standards Institute or ETSI channel 4). The antenna was installed on an electromagnetically transparent plastic support (plastic pylon).

Data from RFID sensor tags were gathered through the RFID reader together with phase data in such a way that, for each phase data entry, a temperature measurement is also recorded.

The measurement started with the antenna at $z_{ant} = 1.34$ m placed at $[2.1, 0, 1.34]^T$m and moved until to reach the point $[0, 0, 1.34]^T$m. Along that path, the antenna is oriented toward the positive y–direction. The second part of the trajectory started with the antenna pointed toward the positive x–direction and placed at $[0, 0, 1.34]^T$m and then moved until $[0, 2.1, 1.34]^T$m. In both cases, the antenna has been moved with a step sampling of 5 cm, which is lower than $\lambda/4 = 8.66$ cm. During the antenna relocations, phase and temperature data were recorded by the reader for signal post-processing. The antenna was moved manually and its location was measured through a laser meter.

TABLE I
UTILIZED TAGS WITH LOCATION

ID	Model	Location	Area	Tripod Material
1	Farsens EVAL02–Hygro–Fenix–RM	$[0.60, 1.80, 1.43]^T$ m	Angled Left	Metallic
2	Confidex Survivor B	$[0.60, 1.80, 1.22]^T$ m	Angled Left	Metallic
3	Farsens EVAL02–Fenix–Vortex–RM	$[1.80, 0.90, 1.14]^T$ m	Angled Right	Wooden
4	Farsens EVAL02–Fenix–Vortex–RM	$[1.80, 0.90, 0.94]^T$ m	Angled Right	Wooden
5	Confidex Survivor B	$[1.20, 1.20, 1.43]^T$ m	Central	Metallic
6	Confidex Survivor B	$[1.20, 1.20, 1.25]^T$ m	Central	Metallic

The RFID sensor tags were distributed within the target area and set on metallic or wooden tripods. In particular, we fixed two tags on each of the three deployed tripods. Each tag was distinguishable by means of its Electronic Product Code (EPC) defined in the local network. Confidex Survivor B tags are optimized to work above metallic surfaces, and therefore were placed directly in contact with the metallic tripods. Farsens tags are characterized by a simple dipole antenna and therefore required a 2-cm thick wooden plate to separate tag antenna from the underneath metallic tripod. Table I shows association between tag number, tag model, location, zone and tripod material. The first tripod was located at an angled location with respect to the target area, and therefore we defined its zone as "Angled Left", the second tripod was at an "Angled Right" location, whereas the last tripod was at a "Central" location. By employing various materials and tag types, the proposed system was validated across different conditions. It is advisable to carefully select suitable tag models when implementing a system like the one suggested in this paper to prevent significant mismatches in RFID tag antenna impedance and a reduction of system performance in terms of reading range and localization accuracy. It is essential to choose RFID tags whit chips incorporating sensing capabilities or supporting external sensors. Additionally, the tag should be able to provide accessible data for remote reading. As for the tag model itself, previous investigations have demonstrated the SAR method effectiveness irrespective of the type of tag used [32].

IV. EXPERIMENTAL RESULTS

A. Localization Performance

The antenna was relocated manually, and $N_M = 250$ phase/temperature readings were gathered at each location. Therefore, N_M different datasets at $N_R = 86$ different antenna locations were collected. SAR localization was performed by exploiting as inputs N_R phase data and the measured antenna trajectory. An example of measured phase when the antenna detects the tag #2 (Confidex Survivor B) in position $\mathbf{p_{tag}} = [x_{tag}, y_{tag}, z_{tag}]^T = [0.60, 1.80, 1.22]^T$ m is depicted in Fig. 4 for two of the $N_M = 250$ test cases. The tag is in "Angled Left" and installed on a metallic tripod.

The phase noise distribution histogram is shown in Fig. 5 for $N_M \times N_R \times N_T = 250 \times 86 \times 6 = 129000$ points, with $N_T = 6$ denoting the number of tags deployed within the room. The distribution is computed by removing the theoretical phase shift caused by the propagation delay and the phase offset. To overcome the phase offset issue, a phase offset

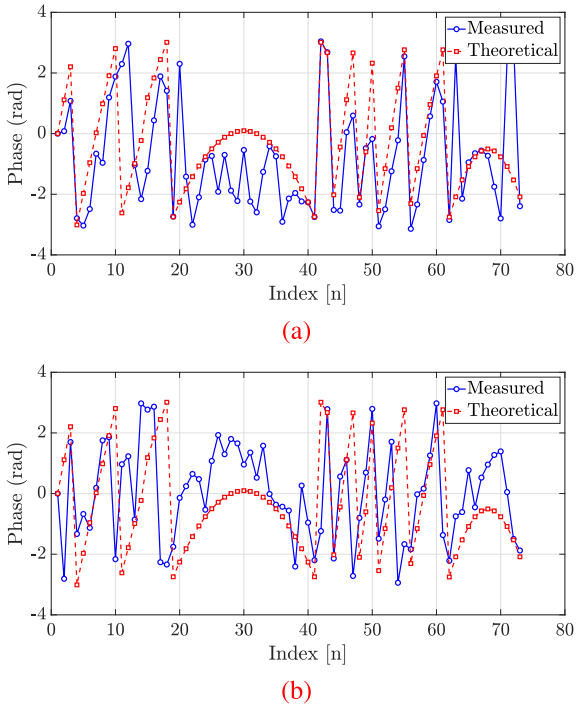

Fig. 4. Phase data gathered by the RFID moving antenna when detecting the tag #2 (Confidex Survivor B) in position $\mathbf{p_{tag}} = [x_{tag}, y_{tag}, z_{tag}]^T = [0.60, 1.80, 1.22]^T$, for two of the $N_M = 250$ test cases: (a) case #1, (b) case #2.

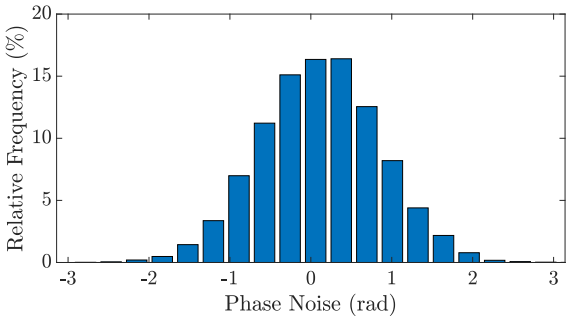

Fig. 5. Histogram of phase noise distribution.

calibration was done on the phase data. The standard deviation of the distribution is $\sigma_w = 0.7$ rad. The residual mean value of the distribution is 0.11 rad, which takes into account the effect of multipath, phase offset variations outside the antenna mainlobe, and non-perfect removal of the propagation delay caused by antenna locations measurement error. As it can be noticed, the distribution resembles a gaussian profile, meaning that high SNR was achieved for the current measurement setup according to the classification made in [35].

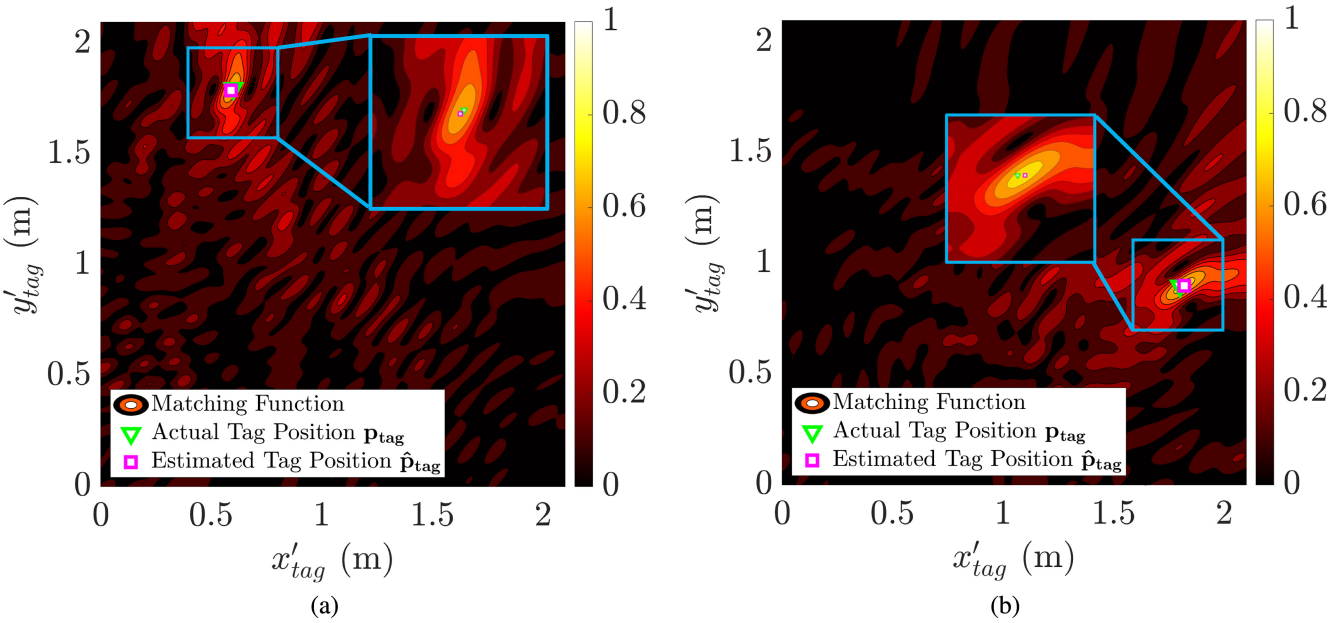

Fig. 6. 2D Matching Function for the xy–plane when $z = z_{tag}$ for two tags: a) when detecting the "Angled Left" tag #2 (Confidex Survivor B) in position $\mathbf{p_{tag}} = [x_{tag}, y_{tag}, z_{tag}]^T = [0.60, 1.80, 1.22]^T$ m; b) when detecting the "Angled Right" tag #4 (Farsens EVAL02–Fenix–Vortex–RM) in position $\mathbf{p_{tag}} = [x_{tag}, y_{tag}, z_{tag}]^T = [1.80, 0.90, 0.94]^T$ m. Actual tag position is represented through triangular green markers, whereas the estimated tag position $\hat{\mathbf{p}}_{\mathbf{tag}}$ is denoted by the squared magenta markers. Lighter colors denotes high values of the matching function.

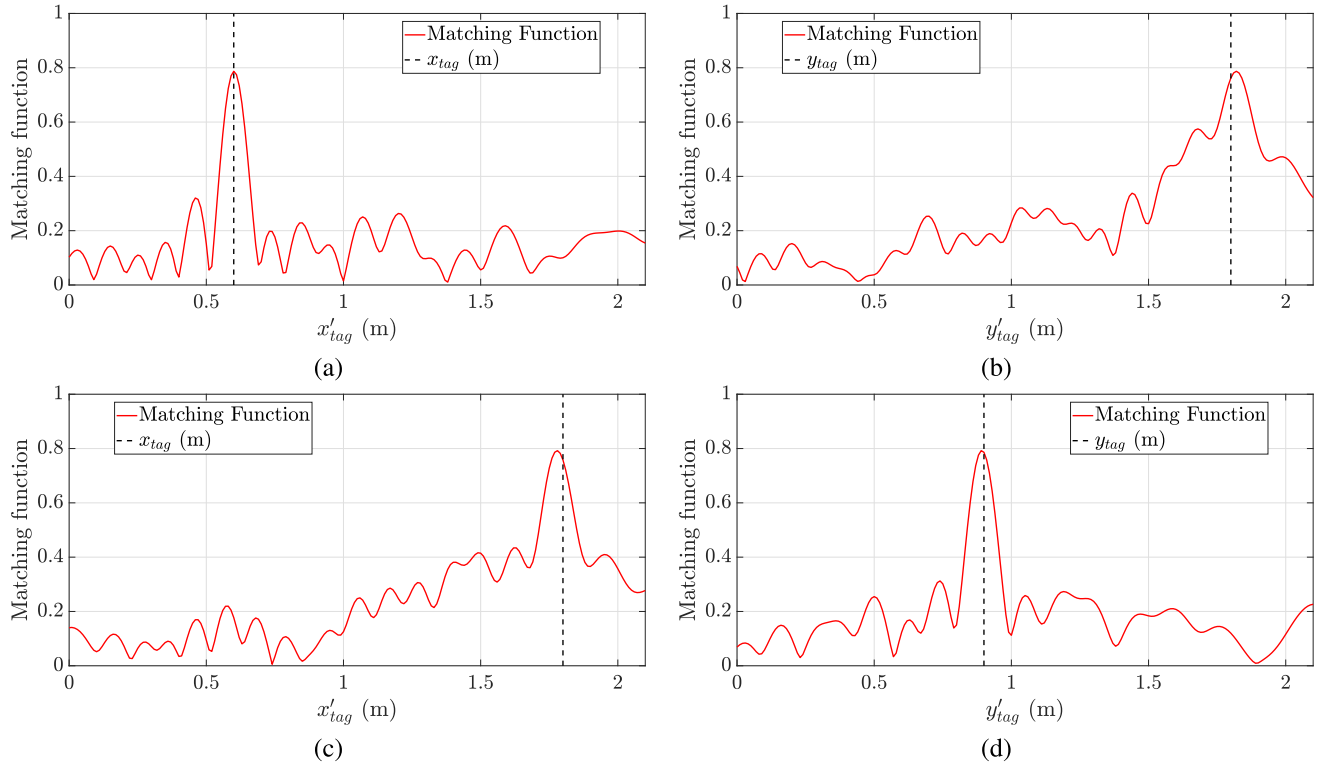

Fig. 7. Single-coordinate Matching Function along the x–axis when $y = \hat{y}_{tag}$ and $z = \hat{z}_{tag}$ for (a) "Angled Left" tag #2 (Confidex Survivor B) in position $\mathbf{p_{tag}} = [x_{tag}, y_{tag}, z_{tag}]^T = [0.60, 1.80, 1.22]^T$ m and for (b) "Angled Right" tag #4 (Farsens EVAL02–Fenix–Vortex–RM) in position $\mathbf{p_{tag}} = [x_{tag}, y_{tag}, z_{tag}]^T = [1.80, 0.90, 0.94]^T$ m. Matching Function along the y–axis when $x = \hat{x}_{tag}$ and $z = \hat{z}_{tag}$ are in (c) and (d) for tag #2 and tag #4, respectively. Actual tag coordinate is drawn with a dashed black line.

The corresponding 2D Matching Function plot for the xy–plane when $z = z_{tag}$ is represented in Fig. 6a. The colormap denotes with lighter colors the higher values of the matching function. The actual tag position is represented through the triangular green marker, whereas the estimated tag position $\hat{\mathbf{p}}_{\mathbf{tag}}$ is denoted by the squared magenta marker and is located through the function peak location. The value of the peak is around 0.8. We define the 2D localization error

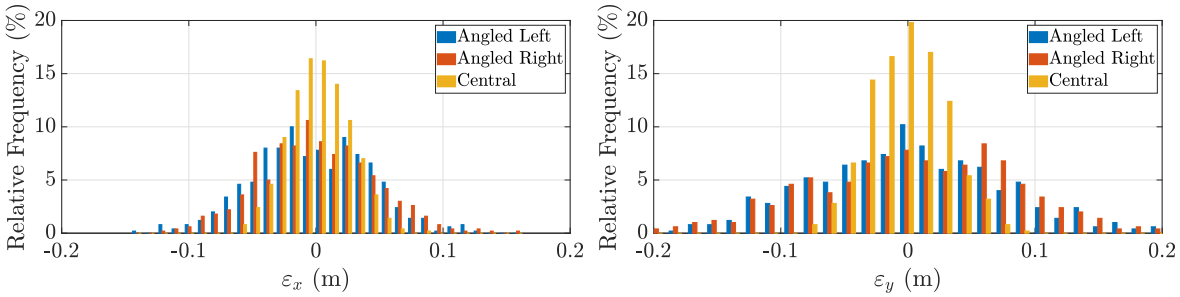

Fig. 8. Histograms of the localization error (a) ε_x and (b) ε_y computed for $N_M = 250$ cases. "Angled Left" tags are in blue, "Angled Right" in red, and "Central" in yellow.

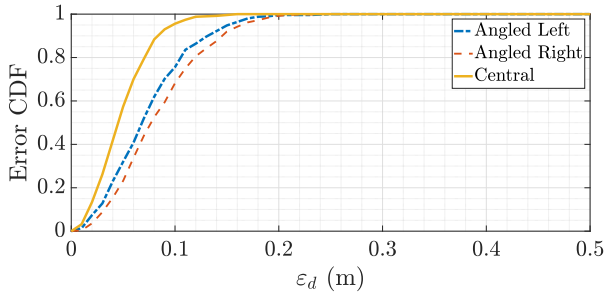

Fig. 9. Cumulative Distribution Function of the Euclidean localization error ε_d computed with $N_M = 250$ cases for "Angled left" (dash-dotted blue line), "Angled Right" (dotted red line), and "Central" (continuous yellow line).

as $[\varepsilon_x, \varepsilon_y]^T = [\hat{x}_{tag} - x_{tag}, \hat{y}_{tag} - y_{tag}]^T$, and consequently an Euclidean distance error $\varepsilon_d = \sqrt{\varepsilon_x^2 + \varepsilon_y^2}$ is defined. For the case described in Fig. 6a, a very accurate tag location was achieved with 4-cm error.

Another example of 2D Matching Function plot is in Fig. 6b. In this case the antenna detects the "Angled Right" tag #4 (Farsens EVAL02–Fenix–Vortex–RM) in position $\mathbf{p_{tag}} = [x_{tag}, y_{tag}, z_{tag}]^T = [1.80, 0.90, 0.94]^T$ m. The 2D matching function is plotted for the xy–plane when $z = z_{tag}$. Good localization performance are obtained also for this different tag model, with different height and location.

Fig. 7a shows the 1D matching function along the x-axis when $y = \hat{y}_{tag}$, and Fig. 7c shows the 1D matching function along the y-axis when $x = \hat{x}_{tag}$ derived from Fig. 6a (Confidex Survivor B). The corresponding tag coordinate is drawn with a dashed black line. The same graphs are represented in Fig. 7b and Fig. 7d for tag #4 Farsens EVAL02–Fenix–Vortex–RM tag and are derived from Fig. 6b. It can be noticed that the mainlobe is relatively thin, by denoting a good resolution of the localization method. In fact, thinner the mainlobe, more accurate the localization [36].

Then, we statistically analyzed the N_M datasets, in order to verify which area among "Angled Left", "Angled Right", and "Central" achieved the best performance in terms of localization error. Due to SAR theory, we expect the "Central" tags to be localized with lower errors.

Fig. 8a shows the histogram of ε_x for the two "Angled Left" (tag #1 and tag #2, blue bars), "Angled Right" (tag #3 and tag #4, red bars), and "Central" (tag #5 and tag #6, yellow bars). It is apparent that the "Central" tags present a thinner error distribution, whereas the angled locations are characterized by a distribution with longer tails. Same considerations hold for the y-coordinate, as shown in Fig. 8b. The computed error mean values and standard deviations highlight that the error distributions are quasi-zero-mean, with standard deviation along x-coordinate $\sigma_x^{AL} = 4.5$ cm, $\sigma_x^{AR} = 4.5$ cm, and $\sigma_x^{C} = 2.4$ cm for "Angled Left" (AL), "Angled Right" (AR), and "Central" (C), respectively, and standard deviation along y-coordinate $\sigma_y^{AL} = 7.4$ cm, $\sigma_y^{AR} = 7.7$ cm, and $\sigma_y^{C} = 3.1$ cm for "Angled Left" (AL), "Angled Right" (AR), and "Central" (C), respectively. A slight unbalance between the standard deviations along x and y might be justified by tag orientations. In fact, all the tags are vertically oriented and facing the direction $-y$, and the radiation pattern on the horizontal plane is not isotropic since the antennas are not ideal dipoles. Therefore, slight differences might appear.

ε_d is indeed a more accurate indicator of system localization performance as it indicates the distance from the actual and estimated tag location. In Fig. 9 we show the Cumulative Distribution Function (CDF) of all the localization errors ε_d for tags at "Angled Left" (dash-dotted blue curve), "Angled Right" (dashed red curve), and "Central" (continuous yellow line) locations. It can be noticed that "Central" locations achieve the lowest estimation errors. Mean errors are $\bar{\varepsilon}_d^{AL} = 7.6$ cm, $\bar{\varepsilon}_d^{AR} = 7.8$ cm, and $\bar{\varepsilon}_d^{C} = 4.9$ cm for "Angled Left" (AL), "Angled Right" (AR), and "Central" (C), respectively. Standard deviations are $\sigma_d^{AL} = 4.1$ cm, $\sigma_d^{AR} = 4.3$ cm, and $\sigma_d^{C} = 2.6$ cm for "Angled Left" (AL), "Angled Right" (AR), and "Central" (C), respectively.

Before delving into a comparison with other localization methods, it is important to remind the distinct architectural advantage of the proposed system based on a SAR technique. Unlike other solutions that rely on different architectures, the proposed system eliminates the need for fixed readers or reference tags. Consequently, making extensive comparisons becomes challenging due to the fundamental differences in infrastructures required by these alternative approaches. However, a comparison of SAR methods is still possible. In [31], it was demonstrated that SAR methods perform similarly to the Maximum Likelihood estimator for high SNR values. It is also pointed out that similar performance will be reached for any SAR method. In this work, we meet the condition of high SNR (see Fig. 5). For the sake of completeness, we mention some solutions that do not rely

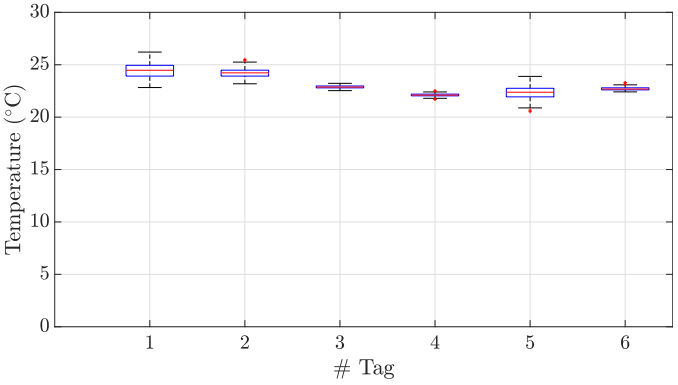

Fig. 10. Boxplot of temperature measured by the RFID sensor tags.

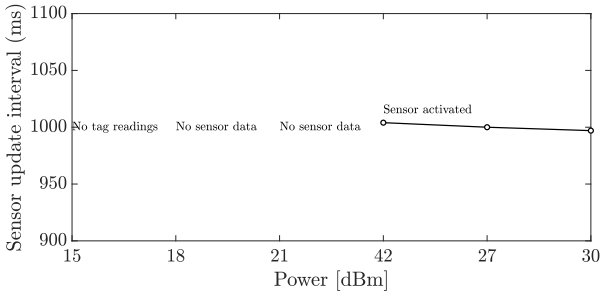

Fig. 11. Sensor update interval of a Farsens EVAL02–Hygro–Fenix–RM tag with varying input power at a distance of 1 m. "No tag readings" and "No sensor data" zones are highlighted with text.

on phasor methods as in this work but on Least-Squares (LS) [28], [37] or hyperbolae intersection optimizations [38], which offer comparable localization performance with reduced processing time and still achieve the same performance for high SNR values. However, phasor-based techniques as the one proposed in this paper may reduce localization errors caused by phase unwrapping issues. Optimized phasor-based SAR techniques exist as the one proposed in [27] or interior point method [39] which will be accounted for future real-time system implementations. Finally, we mention that the localization of RFID sensors could be empowered by means of an Inertial Measurement Unit (IMU) integrated on the RFID sensor tag [8].

B. Sensing Performance

Measured temperature data are shown in the boxplot in Fig. 10. The room temperature was around 24°C. Temperature measurements are not spread, and consecutive tag readings lead to similar measured values.

Then, we tested the ability of the Farsens EVAL02–Hygro–Fenix–RM tag to respond quickly to reader queries and to output a temperature sensor reading (Fig. 11). We placed the tag about 1 m away from the antenna, in a vertical position and both at the same height of 1.34 m. After that, we varied the power delivered by the reader from 15 dBm up to 30 dBm, in 3 dBm steps. It was noticed that a power of 15 dBm is not sufficient to activate the tag chip (Farsens Rocky 100, sensitivity –14 dBm) and thus to read it. With power levels between 18 and 21 dBm the tag responds, but power is not enough to passively power-up the sensor and get temperature data. Above this value, the tag begins to output sensor data, which is updated every 1 second. Higher power slightly increases the update frequency, but the variation is not significant. Given that the tag is read about every 3-4 ms in this configuration, we notice that the temperature readings are replicated many times for different queries. Therefore, we might suggest a reader query routine which foresees to request sensor update at a lower rate than phase readings. Confidex Survivor B tags lead to similar considerations.

We also suggest querying tags from close distances. In fact, this allows to be sure to locate the tag through phase readings and receive at least one sensor reading. In principle, if the antenna is moved by a mobile robot [40], we suggest an initial scan of the environment with an arbitrary trajectory covering as much of the area of interest as possible. Once the RFID tags are located using the SAR method, further scans can be made by setting the vehicle trajectory to approach the tags as closely as possible to retrieve sensor measurements and refine tag location estimations. The distance required depends on the distance at which sensor data can be read in passive mode, and thus on the sensitivity of the chip and the power consumption of the sensing components.

V. Conclusion and Future Works

In this paper we showed a system for environmental mapping based on passive UHF-RFID tags with sensing capabilities. Commercially available RFID sensor tags capable of temperature monitoring are deployed in an indoor scenario. A compact reading system composed by RFID reader and antenna is moved to build an "L-shaped" path which is optimal for 2D tag localization with SAR methods, by leading to average localization errors lower than 5 cm (maximum 20 cm). The reading system can get simultaneously phase and temperature data. Trajectories should be chosen in such a way that target RFID sensor tags do not assume positions that are too sidewise with respect to the antenna path, and distance is limited to ensure sensing data are received. In fact, experimental tests show that sensing in passive mode requires higher power than simple tag identification and therefore lower reader-tag distances are mandatory to maximize the probability of having at least one sensor response. Future works involve the extension of system capabilities to perform real-time operations and the realization of a mobile robotic platform for automatically retrieve phase and sensor data. The robotic platform will perform consecutive runs to update the map status regularly.

References

[1] M. Soori, B. Arezoo, and R. Dastres, "Internet of Things for smart factories in industry 4.0, a review," *Internet Things Cyber-Phys. Syst.*, vol. 3, pp. 192–204, May 2023. [Online]. Available: https://www.sciencedirect.com/science/article/pii/S2667345223000275

[2] B. Yang, J. Tang, X. Dong, S. Li, R. Gu, and J. Hao, "Power inspection design by Internet of Things and RFID technology in smart city," *Microprocess. Microsyst.*, vol. 96, Feb. 2023, Art. no. 104510. [Online]. Available: https://www.sciencedirect.com/science/article/pii/S0141933122000709

[3] A. Mostaccio, G. M. Bianco, G. Marrocco, and C. Occhiuzzi, "RFID technology for food industry 4.0: A review of solutions and applications," *IEEE J. Radio Freq. Identif.*, vol. 7, pp. 145–157, 2023.

[4] L. Catarinucci et al., "An IoT-aware architecture for smart healthcare systems," *IEEE Internet Things J.*, vol. 2, no. 6, pp. 515–526, Dec. 2015.
[5] H. Landaluce, L. Arjona, A. Perallos, F. Falcone, I. Angulo, and F. Muralter, "A review of IoT sensing applications and challenges using RFID and wireless sensor networks," *Sensors*, vol. 20, no. 9, p. 2495, Jan. 2020. [Online]. Available: https://www.mdpi.com/1424-8220/20/9/2495
[6] M. S. Khan, M. S. Islam, and H. Deng, "Design of a reconfigurable RFID sensing tag as a generic sensing platform toward the future Internet of Things," *IEEE Internet Things J.*, vol. 1, no. 4, pp. 300–310, Aug. 2014.
[7] F. Villa-Gonzalez, R. Bhattacharyya, T. Athauda, S. E. Sarma, and N. C. Karmakar, "Detecting breaks in cold chain integrity using chipless RFID time–Temperature sensors," *IEEE Sensors J.*, vol. 22, no. 18, pp. 17808–17818, Sep. 2022.
[8] R. Colella, S. Sabina, P. Mincarone, and L. Catarinucci, "Semi-passive RFID electronic devices with on-chip sensor fusion capabilities for motion capture and biomechanical analysis," *IEEE Sensors J.*, vol. 23, no. 11, pp. 11672–11681, Jun. 2023.
[9] R. Rayhana, G. Xiao, and Z. Liu, "Internet of Things empowered smart greenhouse farming," *IEEE J. Radio Freq. Identif.*, vol. 4, no. 3, pp. 195–211, Sep. 2020.
[10] P. Mezzanotte, V. Palazzi, F. Alimenti, and L. Roselli, "Innovative RFID sensors for Internet of Things applications," *IEEE J. Microw.*, vol. 1, no. 1, pp. 55–65, Jan. 2021.
[11] R. Raju, G. E. Bridges, and S. Bhadra, "Wireless passive sensors for food quality monitoring: Improving the safety of food products," *IEEE Antennas Propag. Mag.*, vol. 62, no. 5, pp. 76–89, Oct. 2020.
[12] S. Benouakta, F. D. Hutu, and Y. Duroc, "UHF RFID temperature sensor tag integrated into a textile yarn," *Sensors*, vol. 22, no. 3, p. 818, Jan. 2022. [Online]. Available: https://www.mdpi.com/1424-8220/22/3/818
[13] S. Dey, O. Salim, H. Masoumi, and N. C. Karmakar, "A novel UHF RFID sensor based crack detection technique for coal mining conveyor belt," *IEEE J. Radio Freq. Identif.*, vol. 6, pp. 19–30, 2022.
[14] F. Costa, S. Genovesi, M. Borgese, A. Michel, F. A. Dicandia, and G. Manara, "A review of RFID sensors, the new frontier of Internet of Things," *Sensors*, vol. 21, no. 9, p. 3138, Jan. 2021. [Online]. Available: https://www.mdpi.com/1424-8220/21/9/3138
[15] F. Zafari, I. Papapanagiotou, and K. Christidis, "Microlocation for Internet-of-Things-equipped smart buildings," *IEEE Internet Things J.*, vol. 3, no. 1, pp. 96–112, Feb. 2016.
[16] Y. Wu, K. Zhang, and Y. Zhang, "Digital twin networks: A survey," *IEEE Internet Things J.*, vol. 8, no. 18, pp. 13789–13804, Sep. 2021.
[17] C. Li, L. Mo, and D. Zhang, "Review on UHF RFID localization methods," *IEEE J. Radio Freq. Identif.*, vol. 3, no. 4, pp. 205–215, Dec. 2019.
[18] A. Motroni, A. Buffi, and P. Nepa, "A survey on indoor vehicle localization through RFID technology," *IEEE Access*, vol. 9, pp. 17921–17942, 2021.
[19] F. Zafari, A. Gkelias, and K. K. Leung, "A survey of indoor localization systems and technologies," *IEEE Commun. Surveys Tuts.*, vol. 21, no. 3, pp. 2568–2599, 3rd Quart., 2019.
[20] J. Xu et al., "The principle, methods and recent progress in RFID positioning techniques: A review," *IEEE J. Radio Freq. Identif.*, vol. 7, pp. 50–63, 2023.
[21] P. V. Nikitin, R. Martinez, S. Ramamurthy, H. Leland, G. Spiess, and K. V. S. Rao, "Phase based spatial identification of UHF RFID tags," in *Proc. IEEE Int. Conf. RFID (IEEE RFID)*, 2010, pp. 102–109.
[22] Y. Ma, H. Liu, Y. Zhang, and Y. Jiang, "The influence of the nonideal phase offset on SAR-based Localization in passive UHF RFID," *IEEE Trans. Antennas Propag.*, vol. 68, no. 8, pp. 6346–6354, Aug. 2020.
[23] A. Buffi et al., "UHF-RFID Localization: The problem of antenna phase center in phase-based methods," in *Proc. 13th Eur. Conf. Antennas Propagat. (EuCAP)*, 2019, pp. 1–5.
[24] A. Motroni, F. Bernardini, A. Buffi, P. Nepa, and B. Tellini, "A UHF-RFID multi-antenna sensor fusion enables item and robot localization," *IEEE J. Radio Freq. Identif.*, vol. 6, pp. 456–466, 2022.
[25] A. Tzitzis et al., "Localization of RFID tags by a moving robot, via phase unwrapping and non-linear optimization," *IEEE J. Radio Freq. Identif.*, vol. 3, no. 4, pp. 216–226, Dec. 2019.
[26] R. Miesen, F. Kirsch, and M. Vossiek, "UHF RFID localization based on synthetic apertures," *IEEE Trans. Autom. Sci. Eng.*, vol. 10, no. 3, pp. 807–815, Jul. 2013.
[27] F. Bernardini et al., "Particle swarm optimization in SAR-based method enabling real-time 3D positioning of UHF-RFID tags," *IEEE J. Radio Freq. Identif.*, vol. 4, no. 4, pp. 300–313, Dec. 2020.
[28] H. Wu, B. Tao, Z. Gong, Z. Yin, and H. Ding, "A fast UHF RFID localization method using unwrapped phase-position model," *IEEE Trans. Autom. Sci. Eng.*, vol. 16, no. 4, pp. 1698–1707, Oct. 2019.
[29] M. Gareis, A. Parr, J. Trabert, T. Mehner, M. Vossiek, and C. Carlowitz, "Stocktaking robots, automatic inventory, and 3D product maps: The smart warehouse enabled by UHF-RFID synthetic aperture Localization techniques," *IEEE Microw. Mag.*, vol. 22, no. 3, pp. 57–68, Mar. 2021.
[30] X. Liang, Z. Huang, S. Yang, and L. Qiu, "E3DinSAR: 3-D localization of RFID-tagged objects based on interference synthetic apertures," *IEEE Internet Things J.*, vol. 7, no. 12, pp. 11656–11666, Dec. 2020.
[31] N. Decarli, "On phase-based localization with narrowband backscatter signals," *EURASIP J. Adv. Signal Process.*, vol. 2018, no. 1, p. 70, Nov. 2018. [Online]. Available: https://doi.org/10.1186/s13634-018-0590-4
[32] A. Buffi, A. Motroni, P. Nepa, B. Tellini, and R. Cioni, "A SAR-based measurement method for passive-tag positioning with a flying UHF-RFID reader," *IEEE Trans. Instrum. Meas.*, vol. 68, no. 3, pp. 845–853, Mar. 2019.
[33] E. D. Giampaolo, F. Martinelli, and F. Romanelli, "The role of the RFID polarization mismatch in the simultaneous localization and mapping problem," *IEEE J. Radio Freq. Identif.*, early access, Jun. 21, 2023, doi: 10.1109/JRFID.2023.3288373.
[34] A. Motroni, A. Ria, L. Strambini, and P. Nepa, "Experimental assessment of passive UHF-RFID sensor tags for environment and kinematic data," in *Proc. IEEE 12th Int. Conf. RFID Technol. Appl. (RFID-TA)*, 2022, pp. 201–204.
[35] M. B. Akbar, D. G. Taylor, and G. D. Durgin, "Amplitude and phase difference estimation bounds for multisensor based tracking of RFID tags," in *Proc. IEEE Int. Conf. RFID (RFID)*, 2015, pp. 105–112.
[36] G. Bandini, A. Motroni, A. Buffi, M. Marracci, and B. Tellini, "On the effect of position uncertainty of the UHF-RFID reader trajectory in SAR-based localization via UAV," in *Proc. IEEE Int. Symp. Meas. Netw. (M&N)*, 2022, pp. 1–6.
[37] A. Tzitzis, A. Malama, V. Drakaki, A. Bletsas, T. V. Yioultsis, and A. G. Dimitriou, "Real-time, robot-based, 3D localization of RFID tags, by transforming phase measurements to a linear optimization problem," *IEEE J. Radio Freq. Identif.*, vol. 6, pp. 439–455, 2022.
[38] P. Tripicchio et al., "A synthetic aperture UHF RFID localization method by phase unwrapping and hyperbolic intersection," *IEEE Trans. Autom. Sci. Eng.*, vol. 19, no. 2, pp. 933–945, Apr. 2022.
[39] G. Bandini et al., "UHF-RFID smart system for worker safety: A hierarchical approach for localization," in *Proc. 7th Int. Conf. Smart Sustain. Technol. (SpliTech)*, 2022, pp. 1–6.
[40] A. Motroni, A. Ria, G. Cecchi, and P. Nepa, "Robot-based UHF-RFID joint SAR localization and tag sensing," in *Proc. 8th Int. Conf. Smart Sustain. Technol. (SpliTech)*, 2023, pp. 1–4.

Andrea Motroni (Member, IEEE) received the M.E. (with Hons.) degree in telecommunication engineering and the Ph.D. (with Hons.) degree in information engineering from the University of Pisa, Pisa, Italy, in 2017 and 2021, respectively, where he is currently an Assistant Professor. In 2019, he was the President of the IEEE Student Branch, University of Pisa. In 2020, he was a visiting Ph.D. student with the Graz University of Technology, Graz, Austria. His current research interests include indoor radiolocalization systems, with specific focus on UHF-RFID and UWB technology for robot and vehicle localization, the integration of robotic systems with RFID toward new systems for industry and logistics, UHF-RFID smart gates and other RFID-based applications for Internet of Things, Industry 4.0., and people safety in both indoor and outdoor environments. He was a recipient of Best Paper Award and Best Student Paper Award at IEEE RFID-TA 2019 and the Young Scientist Award from the International Union of Radio Science, Commission B, in 2018, 2019, and 2021, respectively. In 2022, he was awarded with the IEEE/ABB Italy Section Award for Ph.D. Thesis. In 2022, he was also awarded with the 2021 Best Ph.D. Dissertation in the field of Information and Industrial Engineering from the University of Pisa and with the Best Poster Award at IEEE M&N 2022. In 2023, he was again recognized with Young Scientist Award from the International Union of Radio Science, Commission B, and with Best Poster Award at IEEE RFID 2023. He currently serves as an Associate Editor of the IEEE JOURNAL OF RADIO FREQUENCY IDENTIFICATION. He was a Finalist at the IEEE CRFID Educational Mega Challenge. He has joined the organizing committee and has been the session chair of several IEEE international conferences. He is an Executive Member of the IEEE CRFID's Technical Committee on Motion Capture and Localization.

Glauco Cecchi (Student Member, IEEE) received the M.E. degree in telecommunication engineering from the University of Pisa, Pisa, Italy, in 2020, where he is currently pursuing the Ph.D. degree (Smart Industry) with the Department of Information Engineering, Microwave Research Lab. His research is about passive radio frequency identification systems application in industry 4.0.: he is focusing on applying this technology for the inventory management operations and for radiolocalization in indoor environments.

Andrea Ria (Senior Member, IEEE) received the bachelor's, master's, and Ph.D. degrees in electronics engineering from the University of Pisa, Pisa, Italy, in 2014, 2016, and 2021, respectively, where he is currently an Assistant Professor with the Department of Information Engineering. In 2023 and 2022, he was invited by the University of Perugia, the University of Roma 3, and the Politecnico di Milano to give seminars regarding integrated electronic mixed signal circuits. His research activity is focused on low-voltage and low-power mixed-signal integrated sensor interfaces. In 2019, he won the Distinguished Service Award during the RFID-TA Conference. In 2018, he won the Huawei Italy University Challenge. He is the Vice Chair of the IEEE Student Branch of University of Pisa. He is a TPC Member of RFID-TA Conference and a guest editor of different scientific Journals.

Paolo Nepa (Senior Member, IEEE) received the Laurea degree (summa cum laude) in electronics engineering from the University of Pisa, Pisa, Italy, in 1990. Since 1990, he has been with the Department of Information Engineering, University of Pisa, where he is currently a Full Professor. He is also with the Institute of Electronics, Computer and Telecommunication Engineering, Italian National Research Council, Turin, Italy. In 1998, he was a Visiting Scholar with the Electro Science Laboratory (ESL), The Ohio State University, Columbus, OH, USA, supported by a grant from the Italian National Research Council. At ESL, he was involved in research on efficient hybrid techniques for the analysis of large antenna arrays. He has coauthored more than 300 international journal articles and conference contributions. His research interests are in the design of wideband and multiband antennas for mobile communication systems and antennas optimized for near-field coupling and focusing, as well as in the development of propagation models of wireless radio links for indoor and outdoor scenarios. He is also working on channel characterization, wearable antenna design, and diversity scheme implementation for body-centric communication systems. In the context of UHF-RFID systems, he is working on efficient and accurate techniques for radio localization of either tagged static objects or vehicles, in the Internet of Things and Industry 4.0. scenarios. He was a recipient of the Young Scientist Award from the International Union of Radio Science, Commission B, in 1998. He was a recipient of the Outstanding Associate Editors Awards in 2021. In 2019, he has served as the General Chair for the IEEE RFID-TA 2019, Pisa. Since 2021, he has been serving as an Associate Editor of the IEEE TRANSACTIONS ON ANTENNAS AND PROPAGATION. Since 2023, he has been serving as an Editor-in-Chief of the IEEE JOURNAL OF RADIO FREQUENCY IDENTIFICATION. Since 2016, he has been serving as an Associate Editor of the IEEE ANTENNAS AND WIRELESS PROPAGATION LETTERS. He has served as a TPC member of several IEEE international conferences. Since 2013, he has been a member of the Technical Advisory Board of URSI Commission B—Fields and Waves.

Open Access funding provided by 'Università di Pisa' within the CRUI CARE Agreement